RSC Medicinal Chemistry

ROYAL SOCIETY OF CHEMISTRY

RESEARCH ARTICLE

View Article Online
View Journal | View Issue

Cite this: *RSC Med. Chem.*, 2025, **16**, 2615

Near-infrared photochemical internalization: design of a distorted zinc phthalocyanine for efficient intracellular delivery of immunotoxins†

Mikako Hamabe,[a] Wakako Dewa,[a] Mizue Yuki,[a] Eriko Yamada,[a] Tamako Aiba,[a] Keisuke Horikoshi,[a] Takao Hamakubo,[b] Riuko Ohashi[c] and Akimitsu Okamoto *[a]

Received 28th November 2024,
Accepted 15th March 2025

DOI: 10.1039/d4md00931b

rsc.li/medchem

In the treatment of cancer, the physical and mental stress on patients and the potential for strong side effects are serious problems; therefore, reliable delivery of drugs into cancer tissue cells is required. We have developed a near-infrared (NIR) photosensitizing dye, Zn6PTPc, for NIR-photochemical internalization (PCI) to achieve gentle and efficient endosomal escape and delivery of antibody drugs, which are known to have high targeting ability but low intracellular activity, into target cancer cells. Zn6PTPc allowed longer wavelengths to be used to achieve higher singlet oxygen generation efficiency by the molecular design based on a distorted π-electron system. The system effectively introduced immunotoxins into cells to significantly inhibit tumor tissue growth. The developed potent NIR photosensitizers facilitated NIR-PCI with high tumor-targeting ability.

Introduction

Cancer treatment often causes serious problems due to the high physical and mental burden on the patients and the significant side effects that can be suffered. Photodynamic therapy has recently been investigated as a possible method to avoid these problems. In photodynamic therapy, a photosensitizing dye is injected into the tumor tissue, which is killed by the production of reactive oxygen species upon light irradiation.[1–3] In the treatment of malignant brain tumors, the use of photodynamic therapy in combination with resection improved the 1 year survival rate from 61% to 100%.[4] Photoimmunotherapy has been developed to further improve target selectivity. In this method, a molecule consisting of a photolytic dye IR700DX conjugated to an antibody that binds to an antigen specifically expressed on the surface of tumor cells was used.[5,6] In photodynamic therapy, reactive oxygen species derived from red photosensitizing dyes directly disrupt cell membranes or membrane proteins from the outside of tumor cells, leading to cell death. The use of large amounts of dyes (or antibodies to which dyes are conjugated) that attack cells directly often causes physical strain on the patient, such as photosensitive disorder.

To avoid direct cell attack by photosensitizing dyes, we focused on photochemical internalization (PCI) of anticancer drugs.[7–10] In PCI, the photosensitizing dye is designed to destroy endosomes and release the contained drug into the cytoplasm. The efficacy of the released drug triggers cell death. PCI may solve the problem of low drug efficacy, where the drug is taken into the cell by endocytosis but remains in the endosome and is degraded as a result of fusion with lysosomes (in fact, the efficiency of endosome escape in existing methods is less than 5%[11]). In 2016, a clinical trial (phase 1) was conducted to enhance the efficacy of the anticancer drug bleomycin by PCI with the photosensitizer $TPCS_{2a}$,[12] which resulted in complete tumor disappearance in 58% of patients and tumor reduction in 11% of patients.[8] Thus, it has been suggested that PCI may be able to provide sufficient therapeutic effects for drugs that have previously failed to demonstrate their potential medicinal effects due to low endosomal escape efficiency. On the other hand, to address all the issues associated with photodynamic therapy, a design of photosensitizing dyes suitable for PCI is required. Such a design would require the following features.

[a] *Department of Chemistry and Biotechnology, Graduate School of Engineering, The University of Tokyo, 7-3-1 Hongo, Bunkyo-ku, Tokyo 113-8656, Japan. E-mail: okamoto@chembio.t.u-tokyo.ac.jp*
[b] *Research Center for Advanced Science and Technology, The University of Tokyo, 4-6-1 Komaba, Meguro-ku, Tokyo 153-8904, Japan*
[c] *Division of Molecular and Diagnostic Pathology, Graduate School of Medical and Dental Sciences, Niigata University, 1-757 Asahimachi-dori, Chuo-ku, Niigata 951-8510, Japan*

† Electronic supplementary information (ESI) available: Synthetic methods of Zn6PTPc analogs, NIR light source, absorption wavelength and singlet oxygen quantum yields of conventional photosensitizers, cell viability after addition of immunotoxin and photosensitizers followed by NIR irradiation, and aggregation size of Zn6PTPc. See DOI: https://doi.org/10.1039/d4md00931b

(i) Highly efficient release of singlet oxygen upon irradiation of near-infrared (NIR) light with high tissue permeability.

(ii) Light irradiation of the dye causes damage to the membrane but does not lead to the destruction of eukaryotic cells.

(iii) Cell death is induced by the drug released by photoirradiation, but cells do not die even when the drug is applied in the absence of photoirradiation.

(iv) The dye stays in the affected area and does not circulate in the body, causing internal organ damage or photosensitive disorder.

Several NIR photosensitizers have recently been investigated, such as BODIPY, chlorin, and bacteriochlorin.[13,14] We expected that the photosensitizer candidates would solve the above problem by having a distorted structure of the chromophore planes. The distortion of the chromophore would contribute to an increase in HOMO[15] and would also be expected to reduce aggregation of the dye in solution, which would also contribute to an increase in singlet oxygen quantum yield.[16] The desired photosensitizer may be obtained by introducing substituents in the appropriate positions that induce strain in the chromophore.

In this paper, we report the development of a NIR photosensitizing dye, Zn6PTPc, which enables NIR-PCI (Fig. 1). The dye induces release of singlet oxygen very efficiently upon irradiation with NIR light, thereby effectively introducing immunotoxins into the cells and significantly inhibiting the growth of tumor tissue. The developed competent NIR photosensitizer enabled NIR-PCI with high tumor-targeting ability.

Materials and methods

General

All chemical reactions were conducted in oven-dried glassware under argon. Reaction temperature reported refers to external bath temperature. All solvents and reagents were obtained from commercial suppliers and used without further purification. Thin-layer chromatography was performed on silica gel Merck Kieselgel 60 F_{254} plates and visualized under UV irradiation (λ_{max} = 254 and 365 nm). Column chromatography was carried out with silica gel (63–210 μm) or reverse-phase silica gel (LiChroprep® RP-18, 40–63 μm). UV-vis spectra were recorded with a UV-2550PC (Shimadzu, Japan). Fluorescence spectra were recorded with an RF-5300PC (Shimadzu). ^{1}H and ^{13}C NMR spectra were recorded with a JNM-ECZ600R (JEOL, Japan). Chemical shifts (δ) are quoted in parts per million (ppm) and refer to residual solvent peak. Coupling constants (J) are quoted in hertz (Hz). Electrospray ionization mass spectrometry (ESI-MS) was performed with a microTOF II-NAC (Bruker). Matrix-assisted laser-desorption ionization time-of-flight (MALDI-TOF) mass spectrometry was performed with a microflex-NAC (Bruker). B3LYP/6-31G* calculation was carried out with Spartan 18 ver.1.4.7 (Wavefunction, Inc., USA).

Dulbecco's modified Eagle's medium (DMEM) with L-glutamine and phenol red (Fujifilm, Japan), Ham's F-12 Nutrient Mixture (Sigma Aldrich, USA), fetal bovine serum (FBS) (Biowest, France), 0.25% trypsin–EDTA solution (Thermo Fisher Scientific, USA), phosphate-buffered saline (PBS) (Nissui, Japan), Hoechst dye 33342 (Dojindo, Japan), penicillin–streptomycin (Nacalai Tesque, Japan), and PrestoBlue (Thermo Fisher Scientific) were used for cell culture and cell viability assay. All cell consumables were purchased from AS ONE (Japan) or AGC techno glass (Japan). A431 (human epidermoid carcinoma), A549 (human lung carcinoma), and MCF-7 (human breast carcinoma) were used to determine the cytotoxicity of immunotoxin and Zn6PTPc *in vitro* and *in vivo*. Cell lines were purchased from RIKEN (Saitama, Japan). Cells were cultured in DMEM (Thermo Fisher Scientific) supplemented with 10% FBS, penicillin (100 U mL^{-1}), and streptomycin (0.1 mg mL^{-1}) (Nacalai Tesque). Trypsin (Thermo Fisher Scientific) was used to separate cells from a dish or plate. For absorption measurements in biological assays, a Cytation 5 cell imaging multi-mode reader (BioTek, USA) was used. Microscopic observations were carried out with a LSM510META (Carl Zeiss, Germany).

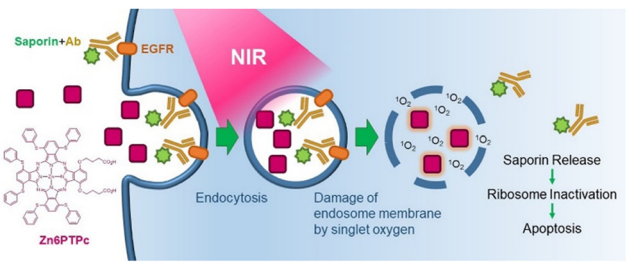

Fig. 1 Target-specific near-infrared photochemical internalization (NIR-PCI) induced by Zn6PTPc.

Synthesis of Zn6PTPc

Compound 2. This compound was synthesized as reported previously.[17] 2,3-Dicyanohydroquinone (**1**) (1.0 g, 6.24 mmol), ethyl 4-bromobutyrate (3.57 mL, 24.9 mmol), and potassium hydroxide (1.75 g, 31.2 mmol) were dissolved in dimethylsulfoxide (30 mL) and stirred at room temperature for 18 h. Water was added to the solution and the precipitate was filtered and washed with water, then dried under reduced pressure to give **2** (2.35 g, 96%). ^{1}H NMR (600 MHz, $CDCl_3$) δ 7.19 (s, 2H), 4.17–4.13 (m, 8H), 2.56 (t, J = 7.0, 4H), 2.15 (quint, J = 6.6, 4H), 1.27 (t, J = 7.2, 6H); ESI-MS m/z [M + Na]$^+$ calcd. 411.1527, found 411.1527.

Compound 3. This compound was synthesized as reported previously.[18] 2,3-Dicyanohydroquinone (**1**) (1.0 g, 6.24 mmol) was dissolved in acetone (8 mL), then *p*-toluenesulfonyl chloride (2.6 g, 13.6 mmol) and potassium carbonate (3.5 g, 25.3 mmol) were added to the solution. The mixture was stirred under reflux for 2 h. After cooling to room

temperature, water was added to the solution and the mixture was stirred for another 1 h at room temperature. The precipitate was collected and washed with water to give **3** (2.86 g, 98%). ^{1}H NMR (600 MHz, DMSO-d_6) δ 7.83 (d, J = 4.1, 4H), 7.81 (s, 2H), 7.42 (d, J = 4.1, 4H), 2.50 (s, 6H); ESI-MS m/z $[M + Na]^+$ calcd. 491.0342, found 491.0346.

Compound 4. This compound was synthesized as reported previously.[18] Tosylated dicyanohydroquinone **3** (1.0 g, 2.13 mmol), potassium carbonate (1.18 g, 8.54 mmol), and thiophenol (0.9 mL, 8.54 mmol, 97% purity) were dissolved in dimethylsulfoxide (25 mL) and the solution was stirred at room temperature for 18 h. Water was added, then the solution was extracted with chloroform and the organic layer was washed with saturated sodium bicarbonate. The organic layer was dried over magnesium sulfate and concentrated *in vacuo*. The crude product was purified by silica gel column chromatography (chloroform/hexane = 3 : 1) to give **4** (411 mg, 56%). ^{1}H NMR (600 MHz, $CDCl_3$) δ 7.49–7.41 (m, 10H), 6.96 (s, 2H); ESI-MS m/z $[M + Na]^+$ calcd. 367.0334, found 367.0334.

Zn6PTPc. Dicyanobenzenes **2** (249.5 mg, 0.64 mmol) and **4** (618.9 mg, 1.8 mmol) were added to a solution of lithium (111.2 mg) in *n*-butanol (10 mL) and the solution was heated under reflux for 2 h. After evaporation to reduce the volume, the mixture was purified by silica gel column chromatography (chloroform/methanol = 9 : 1, containing 1% acetic acid) to give phthalocyanine $H_2$6PTPc (277 mg, 32%) as a black powder. ^{1}H NMR (500 MHz, DMSO-d_6) δ 7.90 (d, J = 6.7, 4H), 7.71 (dd, J = 12.5, 7.0, 8H), 7.61 (dd, J = 13.0, 6.5, 8H), 7.55–7.40 (14H), 7.02–6.85 (4H), 4.64 (t, J = 6.5, 4H), 2.80–2.77 (4H), 2.59–2.54 (4H); MALDI-TOF-MS (α-cyano-4-hydroxycinamic acid) m/z $[M + H]^+$ calcd. 1366.2491, found 1366.9867.

$H_2$6PTPc (29.7 mg, 22 μmol) and zinc acetate (23.9 mg, 0.109 mmol) were dissolved in *N*,*N*-dimethylformamide (2 mL) and the solution was stirred at 100 °C for 5 h. After the solvent was removed *in vacuo*, the residue was purified by silica gel column chromatography (chloroform/methanol = 15 : 1, containing 1% acetic acid) to give Zn6PTPc (20.8 mg, 67%). The product can be stored in a cool, dark place under nitrogen atmosphere for 3 months, although room light and air can induce decomposition of the product. ^{1}H NMR (600 MHz, DMSO-d_6) δ 7.90–6.90 (38H), 4.95–4.50 (4H), 2.70–2.10 (8H, overlap on the solvent signals); ^{13}C NMR (150 MHz, DMSO-d_6) δ 173.81, 171.74, 153.53, 152.68, 151.67, 151.38, 149.62, 135.88, 134.84, 134.43, 133.09, 132.75, 132.64, 132.52, 132.47, 131.69, 131.47, 129.92, 129.87, 129.22, 128.83, 128.63, 126.83, 126.47, 125.98, 125.07, 115.38, 68.56, 30.84, 24.70, 21.27; MALDI-TOF-MS (α-cyano-4-hydroxycinamic acid) m/z $[M + H]^+$ calcd. 1428.1626, found 1428.1641.

Absorption and fluorescence measurements

Absorption and fluorescence spectra were measured in dimethylsulfoxide using a 1 cm path length cuvette with a UV-2550 (UV-visible spectrophotometer). The excitation and emission bandwidths were 1.5 nm. The fluorescence quantum yield (Φ_f) was determined using rhodamine B as a reference, with a known Φ_f = 0.31 in water.

NIR light source

The light source was a MAX-302 (Asahi Spectra, Japan). IR and vis mirror modules (Fig. S1†) were used after the wavelengths below 610 nm were blocked with a LUX filter. According to the MAX303 technical information, the irradiance for a 529 mm^2 area at 700 nm is 9.56 mW cm^{-2}. The irradiation area was 729 mm^2 for cell viability assay and 324 mm^2 for photostability evaluation and confocal microscopy analysis. The absorption maximum of Zn6PTPc was around 780 nm; thus, the irradiance was calculated as 6.1 mW cm^{-2} for cell viability assay and 13.8 mW cm^{-2} for confocal microscopy analysis.

Determination of singlet oxygen quantum yield

The main text of the article should appear here with headings as appropriate. Singlet oxygen quantum yields (Φ_Δ) were determined using the relative method with zinc phthalocyanine (ZnPc) as a reference and 1,3-diphenylisobenzofuran (DPBF) as a chemical quencher for singlet oxygen using the following equation:

$$\Phi_\Delta = \Phi_\Delta^{std} \times \{(R \times I_{abs}^{std})/(R^{std} \times I_{abs})\}$$

where Φ_Δ^{std} is the singlet oxygen quantum yield for ZnPc (Φ_Δ^{std} = 0.67 in dimethylsulfoxide[19]), and R and R^{std} are the DPBF photobleaching rates in the presence of the respective samples and standard, respectively. I_{abs} and I_{abs}^{std} are the rates of light absorption by the samples and standard, respectively.

Hemolysis assay

Fresh blood from mice was centrifuged at 5000 × *g* for 5 min and further washed with PBS five times by centrifugation at 5000 × *g* for 4 min each time. Precipitated blood cells (30 μL) were collected and diluted with 550 μL of PBS. A suspension of Zn6PTPc (80 μL, final concentration of 0.1, 1, 10, and 100 μM) prepared in PBS was added to 20 μL of red blood cell solution in 96-well plates. PBS and water were used as negative and positive controls, respectively. After 100 min of incubation, the samples were irradiated with NIR light (6.1 mW cm^{-2} for 1 h, 22 J cm^{-2}). All the samples were collected and centrifuged at 5000 × *g* for 4 min after 2 h incubation. The 451 nm absorbance of hemoglobin released in the supernatant was measured with a plate reader. The hemolysis percentage was calculated using the following formula:

$$\text{Hemolysis (\%)} = (A - A_{neg})/(A_{pos} - A_{neg}) \times 100$$

where A, A_{pos}, and A_{neg} denote the absorbance values of the sample, the positive control in water, and the negative control in PBS, respectively.

Saporin-modified panitumumab

To a solution of panitumumab (1 mg mL^{-1} in PBS, 50 μL), sulfo-NHS-biotin EZ-link (10 mM, 1.33 μL, 40 eq.) was added and allowed to react at room temperature for 30 min. The conjugate was purified by Microbiospin 6 spin column chromatography. Biotinylated panitumumab and streptavidin–saporin (1 eq.) were mixed on ice for 30 min before use in *in vitro* assays. For *in vivo* experiments, a prepared solution without dilution was stored at −80 °C and used in 2 weeks.

Cell viability assay

Cells (6000 cells per well for MCF-7 and 4000 cells per well for other cells) were seeded onto a 96-well plate and incubated for 24 h. Zn6PTPc at different concentrations and saporin-modified panitumumab (0–32 pM) were added to each well and incubated for another 18 h. The medium was removed under vacuum, and the wells were washed with DMEM twice before adding fresh medium (90 μL). After 3 h incubation, the sample was irradiated with NIR light (6.1 mW cm^{-2} for 25 min per 4 wells, 22 J cm^{-2}). After 48 h, PrestoBlue (10 μL) was added to each well and fluorescence emission (560/590 ± 10 nm) was measured with a plate reader.

Staining with annexin V-FITC and propidium iodide

A431 cells (100 000 cells per well) were seeded on a 12-well plate and incubated for 24 h. Saporin-modified panitumumab (160 pM) and Zn6PTPc (0.1, 1, and 10 μM) were added to each well and incubated for 18 h. The medium was removed under vacuum, and the wells were washed with DMEM, then fresh medium (1000 μL) was added. After 3 h incubation, the sample was irradiated with NIR light (9.9 mW cm^{-2} for 37 min, 22 J cm^{-2}). After 48 h, cells were collected and stained with annexin V-FITC and propidium iodide following the kit protocols by Nacalai Tesque. Fluorescence was measured by flow cytometry (Guava easyCyte, Luminex, Japan) and the measurement was stopped when the cell count reached 10 000.

Animals

BALB/cAJcl-nu/nu female mice (6–8 weeks old) were purchased from Clea Japan.

All animal procedures were performed in accordance with the Guidelines for Care and Use of Laboratory Animals of the University of Tokyo and approved by the Animal Ethics Committee of the University of Tokyo (RAC200005).

In vivo experiments

A549 cells (1×10^7 cells per mouse) were inoculated subcutaneously into the right thighs of the mice. The experiments were initiated when the tumor volume reached approximately 100 mm^3. Mice were randomly divided into four groups (group A, control; group B, Zn6PTPc only; group C, saporin-modified panitumumab only; group D, Zn6PTPc + saporin-modified panitumumab) and 100 μL of PBS (A and B groups) or saporin-modified panitumumab (2 mg kg^{-1} in PBS for groups C and D) was administrated i.p. on day 0. On day 2, 100 μL (including 6.6% DMF) of mouse serum (groups A and C) or Zn6PTPc (1 mg kg^{-1} for groups B and D) was injected intratumorally under anesthesia. After 3 h, each mouse in groups B and D was irradiated under anesthesia with NIR light (22 J cm^{-2}). During irradiation, the whole body except for the tumor area was covered with aluminum foil.

Tumor size and body weight were noted every 2 days. Tumor volume was calculated using the following formula:

$$\text{Volume} = (\text{length}) \times (\text{width})^2/2$$

Histopathological analysis

Tumors were separated from mice after sacrifice and kept in 10% neutral buffered formalin solution (Muto Pure Chemicals, Tokyo, Japan) for 1–2 days. After routine processing and paraffin embedding, tissues were serially sectioned at 3 μm. Sectioned tissues were mounted on slide glasses and stained with hematoxylin and eosin (HE) for histopathological diagnosis.

Results

Design of NIR photosensitizing dye Zn6PTPc

To obtain a dye that efficiently releases singlet oxygen by absorbing light at wavelengths above 750 nm, which is known to have high tissue permeability, we designed a new dye, Zn6PTPc, based on a phthalocyanine photosensitizer. To increase the absorption wavelength of the phthalocyanine ring (Pc ring) (the Q-band of copper phthalocyanine is about 600 nm), electron-donating thiophenyl groups were introduced into the α-positions of the phthalocyanine. Structural calculations (B3LYP/6-31G*) of Zn6PTPc showed a

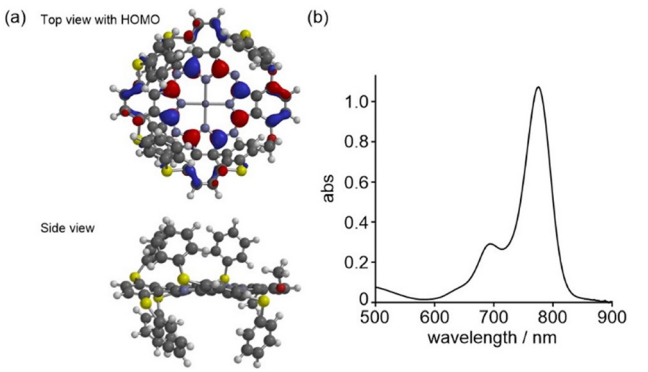

Fig. 2 Calculated structure and vis-NIR absorption spectrum of Zn6PTPc. (a) Top and side view of the structure calculated at the B3LYP/6-31G* level. The carboxylic acid linkers were replaced by methyl groups. HOMO distribution is overlapped onto the top view. (b) Vis-NIR absorption spectrum. The spectrum of Zn6PTPc was measured in dimethyl sulfoxide (10 μM). The absorption maximum in the Q-band is 775 nm and the molar extinction coefficient (ε) at 775 nm is 99 000 M^{-1} cm^{-1} in dimethyl sulfoxide.

distorted Pc ring with a maximum tilt of ±20° from the 4N mean plane due to the proximity between the sulfur atoms at the α-position (Fig. 2a). The distortion of the Pc ring due to substitution at the α-position contributes to the increase of the HOMO–LUMO gap (Table S1†) and it is also expected to prevent the phthalocyanine from aggregating in solution, which would also contribute to increasing the singlet oxygen quantum yield.[16] When the sulfur atom at the α-position was replaced with an oxygen atom, the distortion of the Pc ring was eliminated (a tilt of only about 0.1° for the 4N mean plane). A closed-shell antimagnetic zinc ion was chosen as the metal ion at the center of the Pc ring.[20] In addition, two carboxylic acid modifications were extended from one isoindole unit of phthalocyanine to give the dye moderate solubility in polar solvents. According to the above structural conditions, we have designed a new zinc phthalocyanine molecule, Zn6PTPc.

Facile synthesis of Zn6PTPc

Zn6PTPc was synthesized from 2,3-dicyanohydroquinone (**1**) (Scheme 1). Compound **1** was converted into an ester **2** by condensation with ethyl 4-bromobutyrate.[17] Concurrently, tosylation of **1** and subsequent introduction of thiophenol afforded 1,4-di(thiophenyl)-2,3-dicyanobenzene (**4**).[18] Heating and mixing of dicyanobenzene building units **2** and **4** in a 1 : 3 ratio in 1-butanol in the presence of lithium, followed by stirring in the presence of 5 equiv. of zinc acetate, yielded Zn6PTPc in relatively good yield (21% in two steps). The cyclized byproducts with different building unit ratios were easily removed. To evaluate the structure and function of Zn6PTPc, the S → O substituted **5** and β-substituted **6** of Zn6PTPc were also synthesized by a similar synthetic route[21,22] (Schemes S1 and S2†).

Properties of Zn6PTPc: NIR absorption and singlet oxygen generation

A dark-green solid Zn6PTPc had absorption in the NIR region in dimethyl sulfoxide (Q-band absorption maximum at 775 nm, ε 99 000 M^{-1} cm^{-1} in dimethyl sulfoxide) (Fig. 2b). The singlet oxygen quantum yield of Zn6PTPc was measured to be 0.84 (Table 1), and the log*P* value calculated for $H_2$6PTPc was 0.75. On the other hand, when the sulfur atom of Zn6PTPc was replaced with an oxygen atom (**5**), a shorter absorption maximum (742 nm) and a lower singlet oxygen quantum yield (0.73) were observed (Table 1). The absorption maximum of the Q-band of the β-substituted Zn6PTPc **6** was 725 nm and the singlet oxygen quantum yield was measured to be 0.65. Since the α-position of the Pc ring has a larger molecular orbital coefficient than the β-position, it is known that the introduction of an electron-donating group at the α-position destabilizes the HOMO energy level and shifts the absorption wavelength of phthalocyanine to the longer wavelength side.[15] In addition, the sulfur atoms in **6** are located far from each other between isoindole constituents, which does not lead to distortion of the Pc ring. These structural features of **6** lead to a shorter absorption wavelength and lower singlet oxygen quantum yield in **6** than in Zn6PTPc.

Table 1 Comparison of absorption maxima (λ_{ab}) in the Q-bands and singlet oxygen quantum yields (Φ_Δ) of Zn6PTPc and its analogs

	Zn6PTPc	**5** (O-substitution)	**6** (β-substitution)
λ_{ab}/nm[a]	775	742	725
Φ_Δ[b]	0.84	0.73	0.65

[a] The spectra were measured in dimethyl sulfoxide (10 μM). [b] The quantum yields were determined in dimethyl sulfoxide using the relative method with zinc phthalocyanine as a reference and 1,3-diphenylisobenzofuran as a chemical quencher for singlet oxygen.[19]

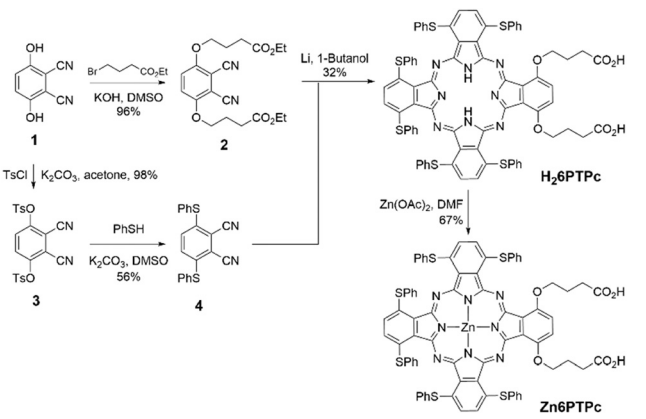

Scheme 1 Synthesis of Zn6PTPc.

Membrane damage caused by NIR light irradiation to Zn6PTPc

The results of hemolysis experiments of erythrocytes showed that the lipid membrane is damaged by the release of singlet oxygen upon irradiating Zn6PTPc with NIR light. We irradiated a solution of Zn6PTPc mixed with mouse erythrocytes in PBS with NIR light (700–1100 nm, 22 J cm^{-2}), and measured the amount of hemoglobin released into the supernatant solution using the absorption at 541 nm. NIR light irradiation of Zn6PTPc caused clear hemolysis of red blood cells (Fig. 3a). As the concentration of Zn6PTPc increased, the percentage of hemolyzed erythrocytes increased. On the other hand, without light irradiation, almost no hemolysis was induced, regardless of the concentration of Zn6PTPc. The results of these hemolysis experiments indicate that Zn6PTPc damaged the membrane using singlet oxygen released by NIR light irradiation.

In the same way, we also tried to test the cytotoxicity by damaging the cancer cell membrane. A431 cells derived from

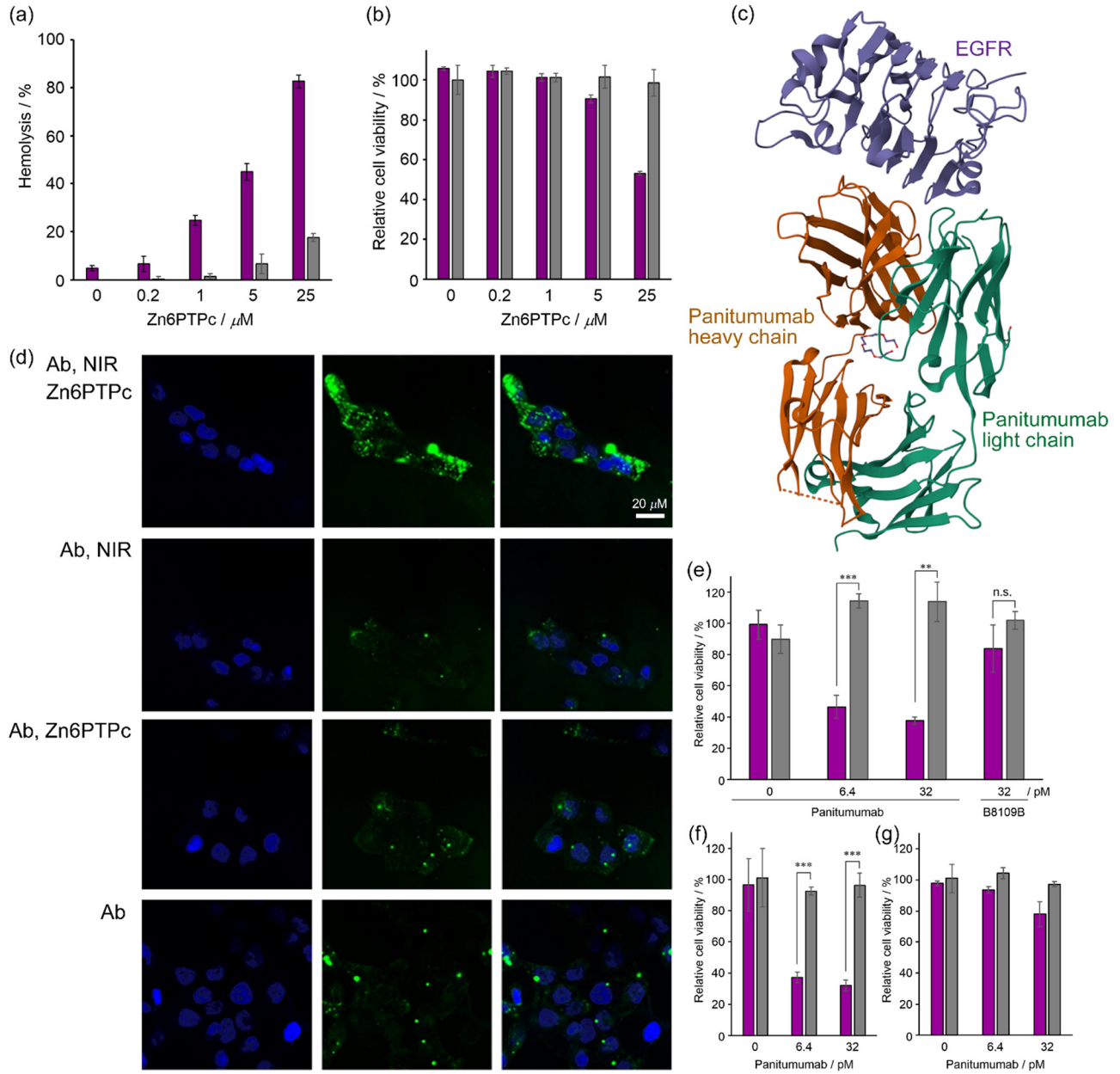

Fig. 3 Membrane damage by NIR irradiation to Zn6PTPc. (a) Hemolysis assay. Zn6PTPc suspension in PBS was added to red blood cell solution in 96-well plates. Exposure to NIR light irradiation (22 J cm^{-2}) after 100 min incubation. Hemolysis efficiency was calculated from the absorbance of released hemoglobin at 541 nm. Each solution of red blood cells in PBS and distilled water without Zn6PTPc was used as negative and positive controls, respectively. Purple, NIR irradiation; gray, in dark. (b) Cytotoxicity of NIR irradiation to Zn6PTPc. A431 cells were irradiated with NIR light (22 J cm^{-2}). After 48 h, fluorescence (560/590 ± 10 nm) from PrestoBlue™ was measured. Purple, NIR irradiation; gray, in dark. The data are displayed in the format of the standard error of the mean (n = 3). (c) Crystal structure of panitumumab in complex with epidermal growth factor receptor (EGFR) domain 3 (PDB ID: 5SX4).[23] Orange, panitumumab heavy chain; green, panitumumab light chain; purple, EGFR domain 3. (d) Confocal microscopy imaging of FITC-modified panitumumab released into A431 cells by treatment with Zn6PTPc. From the top, the addition of FITC-modified panitumumab (1.2 nM) and Zn6PTPc (1 μM) followed by NIR irradiation (16.6 J cm^{-2}), the addition of FITC-modified panitumumab followed by NIR irradiation, the addition of FITC-modified panitumumab and Zn6PTPc, and the addition of FITC-modified panitumumab only. From the left, Hoechst 33342, FITC-modified panitumumab, and merged images. (e)–(g) Cell viability after the NIR-PCI of saporin-modified panitumumab in the presence of 1 μM Zn6PTPc. Purple, NIR irradiation; gray, in dark. The data are displayed in the format of the standard error of the mean (n = 3). **, $p < 0.01$, ***, $p < 0.001$. n.s., not significant. (e) A431 cells. Saporin-modified B8109B does not recognize EGFR. (f) A549 cells. (g) MCF-7 cells.

human epidermoid carcinoma were irradiated with NIR light (22 J cm^{-2}) in the presence of Zn6PTPc, and the reduction in cell viability was limited in the presence of low concentrations (<4 μM) of Zn6PTPc, irrespective of NIR light irradiation (Fig. 3b). Even though Zn6PTPc has membrane-damaging ability as observed in the hemolysis experiment, it

does not have enough membrane-damaging effect to cause the cell death of cancer cells in its low concentration range. In other words, the results of the membrane-damaging experiments described above suggest that Zn6PTPc can be used for the role of temporarily damaging the membranes of intracellular vesicles such as endosomes to release endogenous substances, although it is difficult to use Zn6PTPc to induce a direct cell death mechanism by light irradiation of photosensitizing dyes used in conventional photodynamic therapy.

NIR-PCI with Zn6PTPc

We investigated the release of antibodies taken up into the endosomes of cancer cells upon irradiation of Zn6PTPc with near-infrared light. Epidermal growth factor receptor (EGFR) is a receptor known to be overexpressed in many tumor cells[24] and antibody binding to EGFR is known to induce endocytosis.[25] We observed an efficient cellular uptake of antibodies by NIR-PCI using FITC-labeled anti-EGFR antibody panitumumab (Fig. 3c). FITC (pK_a of *ca.* 6.5) is protonated and fluoresces poorly in acidic environments, such as in endosomes (pH 4.7). The release of FITC-labeled material from endosomes into the cytoplasm is expected to result in strong fluorescence in the cytoplasm.[26–30] After incubation of A431 cells with FITC-labeled panitumumab and Zn6PTPc for 24 h, the cells were washed with culture medium and irradiated with NIR light (16.6 J cm^{-2}). As a result, strong green fluorescence was observed in the entire cytoplasmic region, suggesting that the antibody efficiently escaped from the endosomes and was taken up into the cells (Fig. 3d). However, when either the addition of Zn6PTPc or the irradiation with NIR light was absent, no diffusion of fluorescence in the cytoplasm was observed. Therefore, Fig. 3d shows that Zn6PTPc taken up by endosomes generates singlet oxygen in the endosomes upon irradiation with NIR light, resulting in damage to the endosomal membrane and the release of antibodies into the cytoplasm.

Toxicity to cancer cells induced by NIR-PCI of immunotoxin

The immunotoxin used in this study was obtained by mixing biotinylated anti-EGFR antibody panitumumab with saporin–streptavidin complex. Saporin is known to induce apoptosis and cell death by multiple pathways when taken up into cells.[31] To achieve target selectivity, saporin is conjugated with antibodies, but its efficacy has not been fully demonstrated to date due to its low escape efficiency from endosomes.[32] We incubated A431 cells, which are known to express high levels of EGFR,[33] with a noncytotoxic concentration (1 μM) of Zn6PTPc and saporin-modified panitumumab for 18 h. NIR light irradiation after medium replacement resulted in a dramatic decrease in cell viability (Fig. 3e). Since a noncytotoxic concentration of Zn6PTPc was used and the medium was changed before light irradiation, there was little decrease in cell viability after light irradiation without saporin-modified panitumumab. In addition, when either NIR light or Zn6PTPc was absent, the decrease in cell viability was negligible because saporin-modified panitumumab did not cause endosomal escape. The addition of a mismatched saporin-modified antibody (B8109B) resulted in weak cytotoxicity because of its low level of uptake into endosomes. In other words, the results of this NIR-PCI experiment indicate that Zn6PTPc in the endosomes released singlet oxygen by NIR irradiation, resulting in temporary damage to the endosomal membrane and release of immunotoxin in the endosomes into the cytoplasm, leading to cell death.

A similar NIR-PCI experiment was performed with A549 cells, a human alveolar basal epithelial adenocarcinoma cell line that expresses approximately 10% of the amount of EGFR of A431.[33] Although some studies have used immunotoxins targeting EGFR on A549 cells,[34,35] few studies have shown sufficient cytotoxicity due to the low levels of expression of EGFR. However, irradiation of A549 cells with Zn6PTPc and saporin-modified panitumumab with NIR light reduced cell viability dramatically (Fig. 3f). However, when MCF-7 cells derived from breast cancer, which have been reported to express little EGFR,[36] were treated with Zn6PTPc and saporin-modified panitumumab and irradiated with NIR light, the cytotoxicity was small (Fig. 3g).

Apoptosis induced by NIR-PCI

Efficient introduction of saporin-modified panitumumab into cells by NIR-PCI would result in saporin-induced ribosome inactivation and subsequent cell apoptosis. We performed the staining with annexin V-FITC and PI on A431 cells after NIR-PCI. Light-scattering measurements showed that most of the cells decreased in size after NIR-PCI (Fig. 4a) and that some of the cells were degraded (the plots appearing in the lower left corner of Fig. 4a). Fluorescence measurements of the cells remaining in the gate showed that the cells were moving toward the apoptotic late stage (Fig. 4b, 25% at 1 μM and 50% at 5 μM of Zn6PTPC). The results of FACS analysis suggest that apoptosis was induced by the ribosomal inactivation of saporin toxin introduced into the cells upon NIR-PCI.

Reduction of tumor tissue in model mice by NIR-PCI

We investigated the inhibition of tumor tissue growth by NIR-PCI in A549 graft-bearing mice. Saporin-modified panitumumab was injected into the abdominal cavity of mice with a tumor volume of approximately 100 mm^3, and 2 days later, Zn6PTPc dissolved in mouse serum was injected subcutaneously into the tumor area, since the antibody accumulates on the target cell surface between 24 and 72 h after administration into the body.[37] Three hours later, the mass was irradiated with NIR light (700–1100 nm) from the outside (22 J cm^{-2}). Six days after NIR irradiation, the growth of the mass was clearly inhibited (Fig. 5a). Tumor growth was suppressed in NIR-PCI-treated mice, while tumor growth continued when either or both saporin-modified

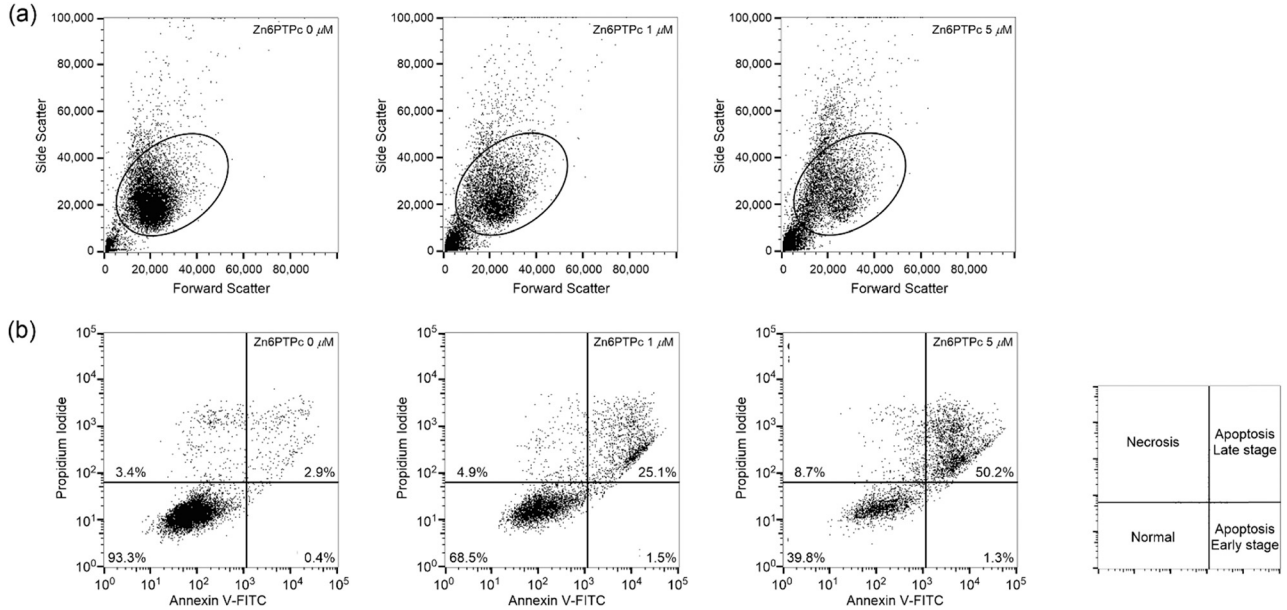

Fig. 4 FACS analysis of A431 cells after NIR-PCI. For NIR-PCI, 160 pM of saporin-modified panitumumab and a range of concentrations of Zn6PTPc (0, 1, and 5 μM from left) were used before NIR irradiation (9.9 mW cm^{-2} for 37 min, 22 J cm^{-2}). (a) Forward and side scatter plots of A431 cells after NIR-PCI. The oval lines in the figures show the gating for (b). (b) Single-cell sorting of A431 cells (cells gated on the oval lines of (a)) stained with annexin V-FITC (*x*-axis) and PI (*y*-axis). The percentages of cells distributed in each region are shown in the figure.

panitumumab and Zn6PTPc were absent (Fig. 5b). The change in body weight of NIR-PCI treated mice after cancer transplantation was within 10% of that of control mice, indicating that the effect of immunotoxin administration and NIR irradiation on body weight was small (Fig. 5c).

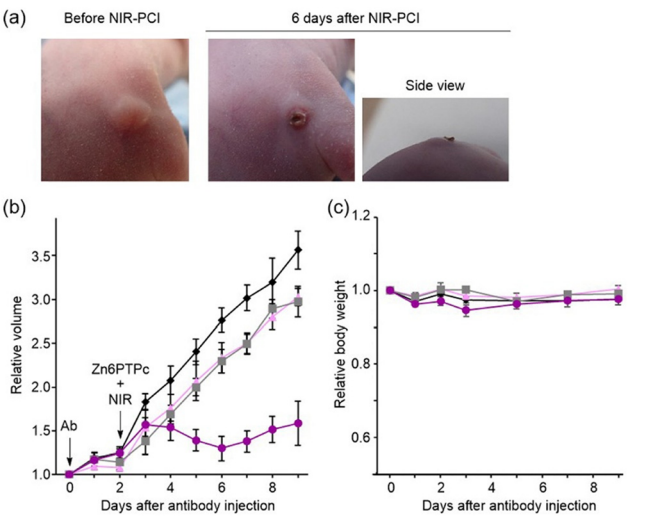

Fig. 5 Reduction of tumor tissue in A549 xenograft nude mice by NIR-PCI. A solution of saporin-modified panitumumab (2 mg kg^{-1}) was injected intraperitoneally, and Zn6PTPc (1 mg kg^{-1}) was injected subcutaneously at the tumor site 2 days later. The surface of the tumor was irradiated with NIR light 3 h later. (a) The difference in appearance between just before injection and 6 days after NIR-PCI. (b) Tumor volume transition. Purple, saporin-modified panitumumab + Zn6PTPc + NIR; light purple, saporin-modified panitumumab; gray, Zn6PTPc + NIR; black, no treatment. The data are displayed in the format of mean ± standard deviation (n = 5). (c) Bodyweight transition. Purple, saporin-modified panitumumab + Zn6PTPc + NIR; light purple, saporin-modified panitumumab; gray, Zn6PTPc + NIR; black, no treatment. The data are displayed in the format of mean ± standard deviation (n = 5).

Histologically, in the group treated with a combination of saporin-modified panitumumab and Zn6PTPc followed by NIR irradiation, most of the tumor mass was replaced by necrosis and inflammatory granulation tissue (Fig. 6). Tumor cells were observed as 'ghost cells' characterized by individualization of cells, increased 'pinkness' of the cytoplasm (hypereosinophilia), and condensed, barely visible nuclei, indicating necrosis (Fig. 6g). A small amount of residual viable tumor cells with polygonal cytoplasm and large, irregular, and oval-to-round nuclei were surrounded by many mononuclear cells with small hyperchromatic round nuclei and divided into small tumor nests (Fig. 6h). On the

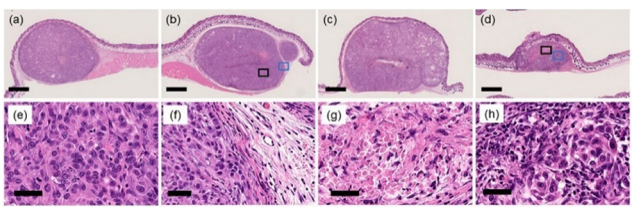

Fig. 6 Hematoxylin and eosin staining of tumor sections after NIR-PCI treatment. (a) No treatment. (b) Saporin-modified panitumumab. (c) Zn6PTPc + NIR. (d) Saporin-modified panitumumab + Zn6PTPc + NIR. (e) Higher-power view of the intratumoral area shown in the black box in section (b). (f) Higher-power view of the intratumoral area shown in the blue box in section (b). (g) Higher-power view of the intratumoral area shown in the black box in section (d). (h) Higher-power view of the intratumoral area shown in the blue box in section (d). Scale bars: 1 mm in (a)–(d); 50 μm in (e)–(h).

other hand, when only saporin-modified panitumumab was added, very few mononuclear cells are observed around the tumor (Fig. 6f). These results suggest that NIR-PCI efficiently induced cancer cells to undergo cell death, and inflammatory cells, including monocytes/macrophages and lymphocytes, were activated to promote the killing of cancer cells, similar to the results reported for other photodynamic therapies.[38–41]

Discussion

Although many photosensitizers have been developed for use in photodynamic therapy, Zn6PTPc has a significant advantage over previous photosensitizers. Zn6PTPc has a higher structural symmetry than the cyclic photosensitizers known in photodynamic therapy, such as photofrin, laserphyrin, and AlPcS2α, so there are fewer combinations of isomeric structures in the products. In addition, the absorption of photosensitizers so far is around 670 nm, which overlaps with that of hemoglobin in the body. The absorption maxima of photofrin (λ_{ab} = 630 nm), laserphyrin (λ_{ab} = 664 nm), and 5-ALA (λ_{ab} = 405 nm for protoporphyrin IX, which results from cytoplasmic metabolism) are all in the visible light range, and their transparency is inferior to that of NIR light. However, the Q-band absorption of Zn6PTPc is 775 nm, more than 100 nm longer than that of laserphyrin. These differences in wavelength imply a two-fold difference in the Rayleigh scattering cross section of light, indicating that light irradiation of Zn6PTPc is more effective for deeper tissues than light irradiation of previous photosensitizers. Furthermore, the distorted ring structure and thiophenyl substituents of Zn6PTPc resulted in high singlet oxygen quantum yields at long wavelengths. Compared with the existing photosensitizers (ZnPc, AlPcS2α, and indocyanine green), Zn6PTPc produced singlet oxygen with outstanding efficiency (Table S1†). The fluorescence quantum yield of Zn6PTPc was only 0.04, suggesting that excited Zn6PTPc can be efficiently converted into the excited triplet state without consuming energy in fluorescence. We also used existing photosensitizers (ZnPc, AlPcS2α, and indocyanine green) as well as Zn6PTPc to irradiate A431 cells with saporin-modified panitumumab with NIR light (700–1100 nm) (22 J cm^{-2}), and no significant decrease in cell viability was observed (Fig. S2†). This may be due to wavelength mismatch and low singlet oxygen release efficiency.

Singlet oxygen is produced by triplet–triplet pairing annihilation between a photosensitizer and an oxygen molecule, which causes oxidative damage to unsaturated lipids close to the region where singlet oxygen is produced (usually within a radius of 20 nm).[42–44] Zn6PTPc trapped in endosomes efficiently generates singlet oxygen upon NIR light irradiation, which damages unsaturated lipids in the endosomal membrane and assists endosomal escape of molecules in the endosome. Efficient endosomal escape of drugs has been studied in the past, and endosomal buffering, which causes endosomal escape in response to pH in the endosome, and membrane-integrated peptide/liposomes using electrostatic interactions have been developed.[45] However, although the efficiency of endosomal escape is improved, time and place selectivity has not been fully achieved. NIR-PCI is an extremely effective means of enhancing the endosomal escape efficiency of molecularly targeted drugs by acting only on the target tumor tissue. It is much milder than the direct damage to cell membranes in conventional photodynamic therapy and is useful as a method of transporting drugs into the cytoplasm of cells irradiated with NIR light.

The moderate solubility of Zn6PTPc is an important key for tumor tissue targeting. Liposoluble phthalocyanine photosensitizers aggregate in water,[46] resulting in weak light absorption and the inability of the photosensitizer to spread throughout the mass when injected into the mass. On the other hand, if it is highly water-soluble, the photosensitizer will circulate in the body and cause the photosensitive disorder. In Zn6PTPc, the log$P$ of Zn6PTPc without zinc ion (H26PTPc) was reduced to 0.75 by adding two carboxyl groups (log$P$ of Pc is 4.79), and it was readily soluble in polar solvents. The size of Zn6PTPc in PBS was suitable for clathrin-mediated endocytosis,[47] although the formation of small aggregates with a diameter of 100 nm was observed (Fig. S3†). Zn6PTPc may form H-aggregates,[48] since it emits little fluorescence as shown above. When Zn6PTPc dissolved in mouse serum was injected subcutaneously at the tumor site, a pale-blue solution of Zn6PTPc spread throughout the mass, and the solution was observed to remain in the mass after injection. Tumor tissue growth was markedly inhibited by NIR light irradiation in the presence of saporin-modified panitumumab injected beforehand. On the other hand, when Zn6PTPc-treated mice were regularly placed under room light, no skin inflammation or rash characteristic of photosensitivity was observed in the skin of the mice, as seen in Fig. 5a.

Our NIR-PCI with Zn6PTPc leaves several approach limitations with respect to the analysis of the mechanism of action. First, the fluorescence intensity of Zn6PTPc is extremely small, unlike previous sensitizers, because Zn6PTPc efficiently uses excitation energy for singlet oxygen generation. Although this is an important advantage of Zn6PTPc, we were not able to observe co-localization of Zn6PTPc with antibodies and endosomes because the light irradiation to obtain the small amount of Zn6PTPc fluorescence degrades endosomes. Although it can be inferred from the changes in tumor tissue that endosomal escape by NIR-PCI occurs in the animal experimental system as in the cellular experimental system, leading to tumor shrinkage, the co-localization is not easy to discuss and is an issue that should be verified by optimizing the timing of administration in future non-clinical studies. The information we currently have on the co-localization of immunotoxins and dyes in animal studies includes the following two points: (i) PET imaging of IgG disposition has been shown by Wu where IgG accumulates most at tumor sites at 24–72 h after intravenous injection;[37] 80% of IgG is

excreted into the bile at 24 h after administration, and the remaining 20% repeatedly enters and leaves the tissues in a metabolic curve with a half-life of several weeks. We have experimented according to this report and obtained valid results. More in-depth pharmacokinetic studies with a longer time and a larger number of mice are needed for the accumulation of the immunotoxins we used in tumors. (ii) As mentioned above, the fluorescence intensity of Zn6PTPc is extremely low, so it is not possible to follow the disposition of Zn6PTPc by fluorescence after intravenous injection. Therefore, at this stage, we chose not to inject Zn6PTPc intravenously, but to inject dark blue Zn6PTPc into the tumor (the injection stains the tumor dark blue) at a time when we expect the immunotoxin to be accumulating on the tissue surface. This allowed us to perform NIR-PCI experiments based on the co-localization of Zn6PTPc and immunotoxins in tumors.

Conclusions

NIR-PCI has been established as a mild and efficient method to guide antibody drugs to endosomal escape and deliver them into cells. Cancer tissue targeting by NIR-PCI was achieved by the moderate solubility of Zn6PTPc, high singlet oxygen generation in the NIR region, receptor recognition of antibody drugs, and by site-specific irradiation with highly penetrating NIR light. Zn6PTPc has realized long-wavelength and high singlet oxygen generation efficiency by the molecular design based on a distorted π-electron system. NIR-PCI of antibody drugs based on Zn6PTPc achieved tumor tissue targeting with fewer side effects than photosensitizers used in conventional photodynamic therapy. Since the NIR-PCI enabled mild endosomal escape of antibody drugs by singlet oxygen, it may be used for the site-selective introduction of other drugs into the body.

Data availability

All the data supporting this study are included in the main text and the ESI.†

Author contributions

A. O. conceived and directed the study. M. H., W. D., M. Y., E. Y., T. A., and K. H. performed the synthetic experiments and analyzed the data. M. H. and W. D. performed the biological experiments and analyzed the data with the aid of T. H. and R. O. All the authors prepared the manuscript.

Conflicts of interest

There are no conflicts to declare.

Acknowledgements

This work was supported by JSPS KAKENHI (18H05504, 21K19040, 23H00317, 23K17969, and 24H02214). We thank J. Kumagai (Histopathology Core Facility, Niigata University Faculty of Medicine) for her outstanding technical assistance.

References

1 D. E. Dolmans, D. Fukumura and R. K. Jain, Photodynamic therapy for cancer, *Nat. Rev. Cancer*, 2003, **3**, 380–387.
2 A. F. dos Santos, D. R. Q. de Almeida, L. F. Terra, M. S. Baptista and L. Labriola, Photodynamic therapy in cancer treatment–an update review, *J. Cancer Metastasis Treat.*, 2019, **5**, 25.
3 G. Gunaydin, M. E. Gedik and S. Ayan, Photodynamic Therapy for the Treatment and Diagnosis of Cancer–A review of the Current Clinical Status, *Front. Chem.*, 2021, **9**, 686303.
4 T. Maruyama, Y. Muragaki, M. Nitta, S. Tsuzuki, T. Yasuda, S. Ikuta and T. Kawamata, Photodynamic Therapy for Malignant Brain Tumors, *Jpn. J. Neurosurg.*, 2016, **25**, 895–904.
5 M. Mitsunaga, M. Ogawa, N. Kosaka, L. T. Rosenblum, P. L. Choyke and H. Kobayashi, Cancer cell-selective in vivo near infrared photoimmunotherapy targeting specific membrane molecules, *Nat. Med.*, 2011, **17**, 1685–1691.
6 X. Xu, H. Lu and R. Lee, Near Infrared Light Triggered Photo/Immuno-Therapy Toward Cancers, *Front. Bioeng. Biotechnol.*, 2020, **8**, 488.
7 K. Berg, P. K. Selbo, L. Prasmickaite, T. E. Tjelle, K. Sandvig, J. Moan, G. Gaudernack, Ø. Fodstad, S. Kjølsrud, H. Anholt, G. H. Rodal, S. K. Rodal and A. Høgset, Photochemical Internalization, *Cancer Res.*, 1999, **59**, 1180–1183.
8 A. A. Sultan, W. Jerjes, K. Berg, A. Høgset, C. A. Mosse, R. Hamoudi, Z. Hamdoon, C. Simeon, D. Carnell, M. Forster and C. Hopper, Disulfonated tetraphenyl chlorin ($TPCS_{2a}$)-induced photochemical internalisation of bleomycin in patients with solid malignancies: a phase 1, dose-escalation, first-in-man trial, *Lancet Oncol.*, 2016, **17**, 1217–1229.
9 S. Oliveira, M. M. Fretz, A. Høgset, G. Storm and R. M. Schiffelers, Photochemical internalization enhances silencing of epidermal growth factor receptor through improved endosomal escape of siRNA, *Biochim. Biophys. Acta, Biomembr.*, 2007, **1768**, 1211–1217.
10 Y. Miyoshi, M. Kadono, S. Okazaki, A. Nishimura, M. Kitamatsu, K. Watanabe and T. Ohtsuki, Endosomal Escape of Peptide-Photosensitizer Conjugates is Affected by Amino Acid Sequences near the Photosensitizer, *Bioconjugate Chem.*, 2020, **31**, 916–922.
11 J.-s. Kim, D.-K. Choi, S.-w. Park, S.-M. Shin, J. Bae, D.-M. Kim, T. H. Yoo and Y.-S. Kim, Quantitative assessment of cellular uptake and cytosolic access of antibody in living cells by an enhanced split GFP complementation assay, *Biochem. Biophys. Res. Commun.*, 2015, **467**, 771–777.
12 K. Berg, S. Nordstrand, P. K. Selbo, D. T. T. Tran, E. Angell-Petersen and A. Høgset, Disulfonated tetraphenyl chlorin ($TPCS_{2a}$), a novel photosensitizer developed for clinical utilization of photochemical internalization, *Photochem. Photobiol. Sci.*, 2011, **10**, 1637–1651.

13 F. Cheng, T. Qiang and T. D. James, Construction and Properties of Strong Near-IR Absorption Photosensitizers, *Adv. Opt. Mater.*, 2024, **12**, 2401012.
14 K. Gogde, S. Kirar, A. K. Pujari, D. Mohne, A. K. Yadav and J. Bhaumik, Near-IR nanolignin sensitizers based on pyrene-conjugated chlorin and bacteriochlorin for ROS generation, DNA intercalation and bioimaging, *J. Mater. Chem. B*, 2025, **13**, 288–304.
15 T. Furuyama, K. Satoh, T. Kushiya and N. Kabayashi, Design, Synthesis, and Properties of Phthalocyanine Complexes with Main-Group Elements Showing Main Absorption and Fluorescence beyond 1000 nm, *J. Am. Chem. Soc.*, 2014, **136**, 765–776.
16 M. A. Revuelta-Maza, S. Nonell, G. de la Torre and T. Torres, Boosting the singlet oxygen photosensitization abilities of Zn(II) phthalocyanines through functionalization with bulky fluorinated substituents, *Org. Biomol. Chem.*, 2019, **17**, 7448–7454.
17 T. Goslinski, T. Osmalek, K. Konopka, M. Wierzchowski, P. Fita and J. Mielcarek, Photophysical properties and photocytotoxicity of novel phthalocyanines – potentially useful for their application in photodynamic therapy, *Polyhedron*, 2011, **30**, 1538–1546.
18 N. Kobayashi, T. Furuyama and K. Satoh, Rationally Designed Phthalocyanines Having Their Main Absorption Band beyond 1000 nm, *J. Am. Chem. Soc.*, 2011, **133**, 19642–19645.
19 J. A. Cardillo, R. Jorge, R. A. Costa, S. M. T. Nunes, D. Lavinsky, B. D. Kuppermann, A. C. Tedesco and M. E. Farah, Experimental selective choriocapillaris photothrombosis using a modified indocyanine green formulation, *Br. J. Ophthalmol.*, 2008, **92**, 276–280.
20 H. Ali and J. E. van Lier, Metal Complexes as Photo- and Radiosensitizers, *Chem. Rev.*, 1999, **99**(9), 2379–2450.
21 T. Furuyama, K. Maeda, H. Maeda and M. Segi, Chemoselective synthesis of aryloxy-substituted phthalocyanines, *J. Org. Chem.*, 2019, **84**, 14306–14312.
22 S. Riebe, C. Vallet, F. van der Vight, D. Gonzalez-Abradelo, C. Wölper, C. A. Strassert, G. Jansen, S. Knauer and J. Voskuhl, Aromatic Thioethers as Novel Luminophores with Aggregation-Induced Fluorescence and Phosphorescence, *Chem. – Eur. J.*, 2017, **23**, 13660–13668.
23 E. A. Sickmier, R. J. M. Kurzeja, K. Michelsen, M. Vazir, E. Yang and A. S. Tasker, The Panitumumab EGFR Complex Reveals a Binding Mechanism That Overcomes Cetuximab Induced Resistance, *PLoS One*, 2016, **11**, e0163366.
24 N. Prenzel, O. M. Fischer, S. Streit, S. Hart and A. Ullrich, The epidermal growth factor receptor family as a central element for cellular signal transduction and diversification, *Endocr.-Relat. Cancer*, 2001, **8**, 11–31.
25 I. H. Madshus and E. Stang, Internalization and intracellular sorting of the EGF receptor: a model for understanding the mechanisms of receptor trafficking, *J. Cell Sci.*, 2009, **122**, 3433–3439.
26 R. F. Murphy, S. Powers and C. R. Cantor, Endosome pH Measured in Single Cells by Dual Fluorescence Flow Cytometry: Rapid Acidification of Insulin to pH 6, *J. Cell Biol.*, 1984, **98**, 1757–1762.
27 A. Marchetti, E. Lelong and P. Cosson, A measure of endosomal pH by flow cytometry in Dictyostelium, *BMC Res. Notes*, 2009, **2**, 7.
28 T. Ohtsuki, S. Miki, S. Kobayashi, T. Haraguchi, E. Nakata, K. Hirakawa, K. Sumita, K. Watanabe and S. Okazaki, The Molecular Mechanism of Photochemical Internalization of Cell Penetrating Peptide-Cargo-Photosensitizer Conjugates, *Sci. Rep.*, 2015, **5**, 18577.
29 Z. ur Rehman, D. Hoekstra and I. S. Zuhorn, Mechanism of Polyplex- and Lipoplex-Mediated Delivery of Nucleic Acids: Real-Time Visualization of Transient Membrane Destabilization without Endosomal Lysis, *ACS Nano*, 2013, **7**, 3767–3777.
30 M. Matsushita, H. Noguchi, Y.-F. Lu, K. Tomizawa, H. Michiue, S.-T. Li, K. Hirose, S. Bonner-Weir and H. Matsui, Photo-Acceleration of Protein Release from Endosome in the Protein Transduction System, *FEBS Lett.*, 2004, **572**, 221–226.
31 L. Polito, M. Bortolotti, D. Mercatelli, M. G. Battelli and A. Bolognesi, Saporin-S6: A Useful Tool in Cancer Therapy, *Toxins*, 2013, **5**, 1698–1722.
32 L. Polito, M. Bortolotti, M. Pedrazzi and A. Bolognesi, Immunotoxins and Other Conjugates Containing Saporin-S6 for Cancer Therapy, *Toxins*, 2011, **3**, 697–720.
33 S. Derer, P. Bauer, S. Lohse, A. H. Scheel, S. Berger, C. Kellner, M. Peipp and T. Valerius, Impact of Epidermal Growth Factor Receptor (EGFR) Cell Surface Expression Levels on Effector Mechanisms of EGFR Antibodies, *J. Immunol.*, 2012, **189**, 5230–5239.
34 C. Deng, J. Xiong, X. Gu, X. Chen, S. Wu, Z. Wang, D. Wang, J. Tu and J. Xie, Novel recombinant immunotoxin of EGFR specific nanobody fused with cucurmosin, construction and antitumor efficiency in vitro, *Onco Targets Ther*, 2017, **8**, 38568–38580.
35 X. Zhou, J. Qiu, Z. Wang, N. Huang, X. Li, Q. Li, Y. Zhang, C. Zhao, C. Luo, N. Zhang, X. Teng, Z. Chen, X. Liu, X. Yu, W. Wu, Y.-q. Wei and J. Li, In vitro and in vivo anti-tumor activities of anti-EGFR single-chain variable fragment fused with recombinant gelonin toxin, *J. Cancer Res. Clin. Oncol.*, 2012, **138**, 1081–1090.
36 R. Shen, D. Ye, Q. Huang, J. Li, Q. Wang and J. Fei, An EGF receptor-targeting amphinase recombinant protein mediates anti-tumor activity in vitro and in vivo, *Acta Biochim. Biophys. Sin.*, 2018, **50**, 391–398.
37 A. M. Wu, Engineered antibodies for molecular imaging of cancer, *Methods*, 2014, **65**, 139–147.
38 M. Korbelik and G. Krosl, Enhanced Macrophage Cytotoxicity against Tumor Cells Treated with Photodynamic Therapy, *Photochem. Photobiol.*, 1994, **60**, 497–502.
39 F. Vanduijnhoven, R. I. Aalbers, J. P. Rovers, O. T. Terpstra and P. J. Kuppen, The Immunological Consequences of Photodynamic Treatment of Cancer, a Literature Review, *Immunobiology*, 2003, **207**, 105–113.
40 A. P. Castano, P. Mroz and M. R. Hamblin, Photodynamic therapy and anti-tumour immunity, *Nat. Rev. Cancer*, 2006, **6**, 535–545.

41 G. Gunaydin, M. E. Gedik and S. Ayan, Photodynamic Therapy—Current Limitations and Novel Approaches, *Front. Chem.*, 2021, **9**, 691697.
42 A. P. Castano, T. N. Demidova and M. R. Hamblin, Mechanisms in photodynamic therapy: part one—photosensitizers, photochemistry and cellular localization, *Photodiagn. Photodyn. Ther.*, 2004, **1**, 279–293.
43 I. O. L. Bacellar and M. S. Baptista, Mechanisms of Photosensitized Lipid Oxidation and Membrane Permeabilization, *ACS Omega*, 2019, **4**, 21636–21646.
44 N. Watabe, Y. Ishida, A. Ochiai, Y. Tokuoka and N. Norimichi Kawashima, Oxidation Decomposition of Unsaturated Fatty Acids by Singlet Oxygen in Phospholipid Bilayer Membranes, *J. Oleo Sci.*, 2007, **56**, 73–80.
45 D. Pei and M. Buyanova, Overcoming Endosomal Entrapment in Drug Delivery, *Bioconjugate Chem.*, 2019, **30**, 273–283.
46 Y. Huang, Y. Liu, Y. Chen, M. Song, M. Huang, J. Xue, L. Liu and J. Li, Probing the interactions of phthalocyanine-based photosensitizers with model phospholipid bilayer by molecular dynamics simulations, *J. Porphyr. Phthalocyanines*, 2018, **22**, 764–770.
47 L. Kou, J. Sun, Y. Zhai and Z. He, The endocytosis and intracellular fate of nanomedicines: Implication for rational design, *Asian J. Pharm. Sci.*, 2013, **8**, 1–10.
48 V. Czikkely, H. D. Försterling and H. Kuhn, Light absorption and structure of aggregates of dye molecules, *Chem. Phys. Lett.*, 1970, **6**, 11–14.

